biomolecules

MDPI

Article

Pyrazolo-triazolo-pyrimidine Scaffold as a Molecular Passepartout for the Pan-Recognition of Human Adenosine Receptors

Veronica Salmaso [1,*], Margherita Persico [2], Tatiana Da Ros [2], Giampiero Spalluto [2], Sonja Kachler [3], Karl-Norbert Klotz [3], Stefano Moro [1] and Stephanie Federico [2,*]

[1] Molecular Modeling Section (MMS), Dipartimento di Scienze del Farmaco, Università di Padova, Via Marzolo 5, I-35131 Padova, Italy; stefano.moro@unipd.it
[2] Dipartimento di Scienze Chimiche e Farmaceutiche, Università degli Studi di Trieste, Via Licio Giorgieri 1, I-34127 Trieste, Italy; margherita.persico@phd.units.it (M.P.); daros@units.it (T.D.R.); spalluto@units.it (G.S.)
[3] Institut für Pharmakologie, Universität of Würzburg, Versbacher Str. 9, D-97078 Würzburg, Germany; sonja.kachler@uni-wuerzburg.de (S.K.); klotz@toxi.uni-wuerzburg.de (K.-N.K.)
* Correspondence: veronica.salmaso@unipd.it (V.S.); sfederico@units.it (S.F.); Tel.: +39-049-827-5801 (V.S.); +39-040-558-3671 (S.F.)

Abstract: Adenosine receptors are largely distributed in our organism and are promising therapeutic targets for the treatment of many pathologies. In this perspective, investigating the structural features of the ligands leading to affinity and/or selectivity is of great interest. In this work, we have focused on a small series of pyrazolo-triazolo-pyrimidine antagonists substituted in positions 2, 5, and N8, where bulky acyl moieties at the N5 position and small alkyl groups at the N8 position are associated with affinity and selectivity at the A_3 adenosine receptor even if a good affinity toward the A_{2B} adenosine receptor has also been observed. Conversely, a free amino function at the 5 position induces high affinity at the A_{2A} and A_1 receptors with selectivity vs. the A_3 subtype. A molecular modeling study suggests that differences in affinity toward A_1, A_{2A}, and A_3 receptors could be ascribed to two residues: one in the EL2, E168 in human A_{2A}/E172 in human A_1, that is occupied by the hydrophobic residue V169 in the human A_3 receptor; and the other in TM6, occupied by H250/H251 in human A_{2A} and A_1 receptors and by a less bulky S247 in the A_3 receptor. In the end, these findings could help to design new subtype-selective adenosine receptor ligands.

Keywords: adenosine receptor; GPCR; molecular modeling; pyrazolo[4,3-*e*][1,2,4]triazolo[1,5-*c*]pyrimidine; antagonists

Citation: Salmaso, V.; Persico, M.; Da Ros, T.; Spalluto, G.; Kachler, S.; Klotz, K.-N.; Moro, S.; Federico, S. Pyrazolo-triazolo-pyrimidine Scaffold as a Molecular Passepartout for the Pan-Recognition of Human Adenosine Receptors. *Biomolecules* **2023**, *13*, 1610. https://doi.org/10.3390/biom13111610

Academic Editors: Fabrizio Vincenzi, Katia Varani, Stefania Merighi and Stefania Gessi

Received: 25 September 2023
Revised: 24 October 2023
Accepted: 30 October 2023
Published: 3 November 2023

1. Introduction

The effects of adenosine are mediated through a family of cell-surface G-protein-coupled receptors, which are currently classified into four adenosine receptor subtypes: A_1, A_{2A}, A_{2B}, and A_3. While the A_1 and A_3 receptors interact with G_i and G_o proteins, the mechanism of the A_{2A} and A_{2B} subtypes is the stimulation of adenylyl cyclase via G_s proteins. The consequences of these interactions are a reduction, in the case of A_1 and A_3, or an increase, in the case of A_{2A} and A_{2B}, in the cAMP levels as the second messenger. In addition, all four subtypes may positively couple to phospholipase C via different G-protein subunits [1–4]. It has also been demonstrated that adenosine receptors can activate different signal pathways not related to G proteins, like the β-arrestin one, which induces different responses with respect to the G-protein signals [3].

Considering the large distribution of adenosine in the organism, it is quite evident that adenosine receptors could be considered an important target for the treatment of several pathologies. In fact, in the last decades, different classes of potent and selective agonists and antagonists have been reported with the aim of characterizing and better understanding

the pathophysiological role of adenosine receptor subtypes and their possible involvement in several disorders [5–11]. In particular, A_1 antagonists are investigated for their effect on both cardiovascular and metabolic diseases [7]; A_{2A} and A_{2B} antagonists are attracting increasing attention as cancer immunotherapy agents, while A_{2A} is also under study for the treatment of neurodegenerative disorders (i.e., istradefylline is already approved as adjunctive therapy to levodopa in Parkinson's disease) [9,10]; and, finally, A_3 antagonists proved effective in preclinical animal models of brain ischemia and oxygen–glucose deprivation in hippocampal slices [6–11]. Despite the undoubtedly therapeutic potential of these ligands, only istradefylline has been approved in the last years. The biggest problem of adenosine receptors is that adenosine signaling is almost ubiquitous in our body, leading to a very broad spectrum of effects that, at a therapeutic level, could lead to several unpleasant side effects [6]. The pyrazolo-triazolo-pyrimidine nucleus substituted in positions 2, 5, N7, and N8 has already been detected as one of the representative scaffolds among human adenosine receptor antagonists [12–14].

In fact, it has been widely reported that by modulating the pattern of substitutions, in particular, at positions 5, N7, and N8, various compounds with different profiles of affinity and selectivity toward the four adenosine receptor subtypes have been obtained [15]. The aim of this work is to try to better explain with the help of computational methodologies the influence of these patterns of substitutions on both affinity and selectivity vs. adenosine receptor subtypes. In particular, highlighting the specific residues in the four adenosine receptors that are probably responsible for the observed compounds' affinity profile could not only help rationalize the obtained results of these compounds and others already reported in the literature, but it could also aid the design of new potent and selective ligands.

2. Materials and Methods

2.1. Computational Methodologies

The molecular modeling studies have been accomplished on a workstation equipped with a 20-core Intel Core i9-9820X 3.3 GHz processor and by running Ubuntu 20.04 as operating system.

2.1.1. Protein Preparation

X-ray structures with PDB IDs 5UEN [16] and 4EIY [17] were retrieved for hA_1 AR and hA_{2A} AR. The structures were pre-processed by removing apocytochrome b(562)RIL, replacing IL3, and reverting mutations of the crystal construct into wild type. The structures were then prepared with the Structure Preparation tool of the Molecular Operating Environment (MOE) 2022.02 suite [18] by adding missing atoms/residues/loops and capping N/C-terminals (which were not reconstructed) with acetyl and N-methyl group. Protomeric and tautomeric states were optimized with the Protonate3D tool, and hydrogens were then minimized with Amber 14:EHT force field. Non-protein atoms were removed. The Na^+ ion, acting as negative allosteric modulator [19], and three coordination water molecules, co-crystallized to hA_{2A} AR on structure 4EIY, were kept for docking studies. Na^+ and water molecules were also aligned to hA_1 AR structure, minimized, and kept for further modeling. The influence of Na+ on antagonists' docking was assessed before, showing how the posing accuracy is affected by the presence of Na^+ [20].

Structures for hA_{2B} and hA_3 AR were built by homology modeling using the prepared structures of hA_{2A} and hA_1 AR, respectively. Extracellular Loop 2 (EL2) (from residue N145 to residue G160) was removed from the A_{2A} AR structure template (4EIY). The models were generated using Prime of the Schrödinger suite [21,22] with knowledge-based setting and keeping ligands, Na^+, and the three selected water molecules as modeling environment. Non-conserved residues were minimized with OPLS4 force field.

The Ballesteros–Weinstein GPCR numbering scheme, based on counting residues from the most conserved positions in each transmembrane helix (TM), has been employed throughout the manuscript and extracted from the GPCRdb website [23,24].

2.1.2. Molecular Docking

Molecular docking was carried out using Glide [25]. A grid centered on F171/168/173/168 (EL2) and N254/253/254/250 (N6.55) for $hA_1/hA_{2A}/hA_{2B}/hA_3$, respectively, was built for all the receptor structures, with inner and outer box dimensions of 10 Å and 30 Å, respectively. Glide-SP [25] was employed for docking, including the "enhance planarity of conjugated pi groups" setting.

In order to enable docking of bulky compounds (**1**–**7**), an induced-fit docking procedure was employed, using compound **4** as reference (the bulkiest compound with reported binding affinity for all AR subtypes). In particular, the induced-fit docking tool of the Schrödinger package was used [26], optimizing side chains within 5 Å of the docking poses and using SP as scoring function for Glide redocking. The trimming option was included for side chains of residues occluding the binding pocket such as $E172^{EL2}$, $M177^{5.35}$, and $T270^{7.35}$ in the case of hA_1 AR; $E169^{EL2}$, $M174^{5.35}$, $H264^{EL3}$, and $M270^{7.35}$ in the case of hA_{2A} AR; $E174^{EL2}$, $M179^{5.35}$, $N266^{EL3}$, and $M272^{7.35}$ in the case of hA_{2B} AR; and $V169^{EL2}$, $M174^{5.35}$, $I253^{6.58}$, and $L264^{7.35}$ in the case of hA_3 AR. A refined structure was selected for each receptor with visual inspection (bidentate H-bond with N6.55) and used for Glide-SP docking of compounds **1**–**7**.

Docking results were filtered by excluding poses with positive ligand–receptor van der Waals and electrostatic interaction potential (computed in MOE with Amber 14:EHT force field and assigning PM3 partial charged to ligands). Poses were ranked on the basis of electrostatic interaction potential, and one or two poses per compound were selected, prioritizing diverse conformations showing a bidentate hydrogen bond (or approximate one) with N6.55 using visual inspection.

The selected poses are reported in Videos S1–S4 generated using a Python script and the following tools: UCSF Chimera for 3D structure representation [27], MOE for per-residue electrostatic and hydrophobic interaction computation, Gnuplot for heat-map plotting, MEncoder for video assembly.

2.2. Chemistry

Synthesis and characterization of compounds **1**–**7** have already been reported in the literature [28,29]; for new experiments on A_{2B} receptor, the same batch of compounds **1**–**4** synthetized before have been used. Briefly, as reported in Scheme 1, the 8-alkyl-2-(furan-2-yl)-8*H*-pyrazolo[4,3-*e*][1,2,4]triazolo[1,5-*c*]pyrimidin-5-amine derivatives **8**–**12** were reacted with the corresponding acylchloride in the presence of triethylamine, affording compounds **1**–**7**.

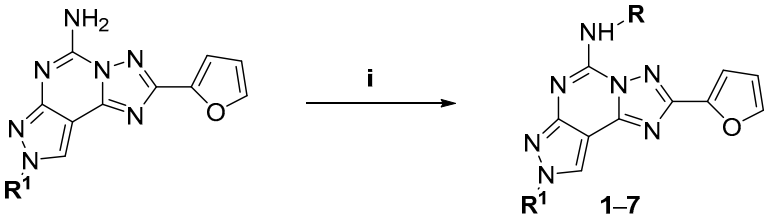

$R^1 = CH_3$, **8**;
$R^1 = C_2H_5$, **9**;
$R^1 = nC_3H_7$, **10**;
$R^1 = nC_4H_9$, **11**;
$R^1 = CH_2CH_2CH(CH_3)_2$, **12**

R = $COCHPh_2$ $R^1 = CH_3$, **1**;
R = $COCHPh_2$ $R^1 = C_2H_5$, **2**;
R = $COCHPh_2$ $R^1 = nC_3H_7$, **3**;
R = $COCHPh_2$ $R^1 = nC_4H_9$, **4**;
R = $COCHPh_2$ $R^1 = CH_2CH_2CH(CH_3)_2$, **5**;
R = $COCH_2$-2-thienyl $R^1 = C_2H_5$, **6**;
R = $COCH_2$-2-thienyl $R^1 = CH_3$, **7**

Scheme 1. Synthesis of compounds **1**–**7**. Reagents and Conditions: i: RCOCl, TEA, THF, reflux, 18 h.

2.3. Biology

2.3.1. Binding at Human A_1, A_{2A}, A_{2B}, and A_3 Adenosine Receptors

All pharmacological methods followed the procedures described earlier [30]. In brief, membranes for radioligand binding were prepared from CHO cells stably transfected with human adenosine receptor subtype (obtained as reported in reference [30]) in a two-step procedure. In a first low-speed step (1000× *g*), cell fragments and nuclei were removed. The crude membrane fraction was sedimented from the supernatant at 100,000× *g*. The membrane pellet was resuspended in the buffer used for the respective binding experiments, frozen in liquid nitrogen, and stored at −80 °C.

Compounds were dissolved in DMSO and then diluted to the desired concentration in buffer, and at least 6 different concentrations were tested. DMSO in the final solution never exceeded 2%. For radioligand binding at A_1 adenosine receptors, 1 nM [^{3}H]CCPA was used, whereas 30 and 10 nM [^{3}H]NECA were used for A_{2A} and A_3 receptors, respectively. Non-specific binding of [^{3}H]CCPA was determined in the presence of 1 mM theophylline; in the case of [^{3}H]NECA, 100 μM R-PIA was used [30,31]. For radioligand binding assay of compounds **1**–**4** at A_{2B} receptors, membranes (20 μg membrane protein) were incubated in a total volume of 200 μL (assay buffer: Tris/HCl pH 7.4, 10 mM $MgCl_2$, 0.1% bovine serum albumin) with 10 nM [^{3}H]ZM241385. Non-specific binding of [^{3}H]ZM241385 was determined in the presence of 0.3 mM NECA. After 3 h at room temperature, samples were filtered and washed as described [31]. K_i values from competition experiments were calculated with the program SCTFIT [32] and represented the mean of 3–6 replicates with 95% confidence limits. Binding data for compounds **1**–**12** at the A_1, A_{2A}, and A_3 adenosine receptors were taken from our previous works [28,29,33]. Binding data toward A_{2B} receptors for compounds **8**–**12** were already reported in a previous work following a different procedure [33].

2.3.2. Adenylyl Cyclase Activity in CHO Cells Expressing hA_{2B} Receptors

Functional studies for the hA_{2B} adenosine receptors were performed using adenylyl cyclase experiments. Minor modifications were carried out on the previously reported procedures [30,34]. In this experimental procedure, the homogenate of hA_{2B}-CHO cells was subjected to high-speed centrifugation, and the sedimented membrane pellet was then resuspended in buffer (50 mMTris/HCl pH 7.4) and directly used for the assay. IC_{50} values of antagonists were determined by their concentration-dependent inhibition of NECA-stimulated adenylyl cyclase activity (NECA, 5 μM). About 150,000 cpm of [α-^{32}P]ATP was incubated with membranes and the incubation mixture for 20 min without EGTA and NaCl [34]. Hill equation was used to calculate IC_{50} which was the mean of 3–6 replicates. Hill coefficients were near unity.

3. Results

As depicted in Table 1, all the compounds showed affinities in the nanomolar range at the four adenosine receptor subtypes with different levels of selectivity. An appropriate discussion regarding the structure–activity relationship profiles of these compounds has been extensively reported [13–15,33]; nevertheless, a brief summary may be necessary to better understand the computational studies.

It is quite evident that the simultaneous introduction of bulky acyl moiety at the N5 position and small alkyl groups at the N8 position led to derivatives (e.g., compounds **1**, **2**) with high affinity at the A_3 adenosine receptor (AR) with good levels of selectivity vs. the other receptor subtypes. The increasing size of the N8 substituent (e.g., compound **5**) led to a significant reduction in affinity at the A_3 subtype with a reduction in the levels of selectivity. It should be otherwise noted that this pattern of substitution led also to a good affinity at the A_{2B} ARs (compounds **1**–**4**), but the highest affinity was still retained at the A_3 subtype. Instead, the introduction of thienyl moiety at the N5 position (e.g., compound **6**) induced a reduction in both affinity and selectivity for the A_3 AR subtype.

Table 1. Biological profile at the four human adenosine receptor subtypes of the pyrazolo-triazolo-pyrimidine compounds **1–12**. R and R^1 refer to general structure depicted in Scheme 1. All data were already reported by Baraldi et al. (**8–12**) [33] and Michielan et al. (**1–7**) [28,29], except for binding data at hA_{2B} receptor for compounds **1–4** which are reported for the first time in this work.

Compd	R	R^1	hA_1 (Ki nM) [1]	hA_{2A} (Ki nM) [2]	hA_{2B} (Ki nM)	hA_{2B} (IC_{50} nM) [5]	hA_3 (Ki nM) [6]
1	$COCHPh_2$	CH_3	139 (82.7–235)	216 (152–307)	29.1 [3] (22.8–37.1)	363 (318–414)	0.25 (0.15–0.41)
2	$COCHPh_2$	CH_2CH_3	156 (102–239)	131 (127–135)	18.3 [3] (11.8–28.2)	745 (482–1150)	0.98 (0.54–1.75)
3	$COCHPh_2$	$CH_2CH_2CH_3$	80.2 (49.7–129)	46.5 (38.2–56.5)	13.3 [3] (5.71–30.8)	491 (327–736)	0.93 (0.69–1.25)
4	$COCHPh_2$	$CH_2CH_2CH_2CH_3$	129 (92.6–180)	114 (81.3–159)	11.5 [3] (8.17–11.3)	780 (650–936)	1.20 (0.74–1.94)
5	$COCHPh_2$	$CH_2CH_2CH(CH_3)_2$	441 (281–692)	159 (136–188)	n.d.	>10,000	5.86 (3.34–10.3)
6	$COCH_2$-2-thienyl	CH_2CH_3	148 (116–189)	15.9 (8.24–30.8)	n.d.	>10,000	196 (160–241)
7	$COCH_2$-2-thienyl	CH_3	444 (390–505)	56 (26.7–117)	n.d.	>10,000	5.26 (3.70–7.47)
8	H	CH_3	101 (81–127)	2.80 (2.40–3.55)	90 [4] (81–101)	n.d.	300 (265–339)
9	H	CH_2CH_3	5.00 (4.05–6.20)	1.95 (1.70–2.10)	65 [4] (56–75)	n.d.	331 (285–385)
10	H	$CH_2CH_2CH_3$	10 (7–14)	2.51 (1.90–3.37)	39 [4] (35–45)	n.d.	408 (364–460)
11	H	$CH_2CH_2CH_2CH_3$	14 (11–17)	1.60 (1.4–2.1)	53 [4] (40–69)	n.d.	600 (525–691)
12	H	$CH_2CH_2CH(CH_3)_2$	2.00 (1.72–2.36)	0.78 (0.60–1.00)	9.1 [4] (7.4–11.3)	n.d.	700 (664–738)

[1] Displacement of specific [^{3}H]CCPA binding at human A_1 receptors expressed in CHO cells. [2] Displacement of specific [^{3}H]NECA binding at human A_{2A} receptors expressed in CHO cells. [3] Displacement of specific [^{3}H]ZM241385 binding at human A_{2B} receptors expressed in CHO cells. [4] Displacement of specific [^{3}H]DPCPX binding at human A_{2B} receptors expressed in HEK-293 cells. [5] IC_{50} values of the inhibition of NECA-stimulated adenylyl cyclase activity in CHO cells expressing hA_{2B} receptors. [6] Displacement of specific [^{3}H]NECA binding at human A_3 receptors expressed in CHO cells. Data are expressed as geometric means with 95% confidence limits; n.d. = not determined.

In contrast, the derivatives with the free amino function at the 5 position induced a different pattern of affinity. In fact, all the compounds showed high affinity (0.8–2.8 nM) at the A_{2A} AR without selectivity vs. the A_1 and A_{2B} subtypes while possessing affinity in the high nanomolar range (300–700 nM) at the human A_3 AR, confirming the fundamental role of the bulky substituent at the N5 position for A_3 AR recognition and the free amino function for A_{2A}/A_1 interaction.

With the aim of rationalizing this behavior, we performed molecular modeling studies investigating the capability of these compounds to assume a reasonable bound state at the orthosteric binding pocket of the hA_1, hA_{2A}, hA_{2B}, and hA_3 ARs.

The four AR subtypes share a high sequence identity, with values ranging around 40% (Table S1). In particular, hA_1 AR shares 46% residues with hA_3 AR, 43% with hA_{2B} AR, and 38% with hA_{2A} AR, with sequence similarity values above 48% in all cases (see Table S1). Moreover, hA_{2A} AR has a 45% sequence identity with hA_{2B} AR and 30% with hA_3 AR, which shares 35% residues with hA_{2B} AR. Most of the dissimilarities are located in the extracellular and intracellular loop regions, with transmembrane (TM) helices having even higher similarities (the TM sequence identity being between a minimum of 45% (A_{2B}/A_3) and a maximum of 66% (A_{2A}/A_{2B}), see Table S1).

The availability of X-ray tridimensional (3D) structures for the antagonist-bound A_{2A} and A_1 ARs in the inactive state provided a starting point for the modeling studies. In

particular, structures with PDB code 4EIY [17] and 5UEN [16] were used for the hA_{2A} and hA_1 ARs, respectively. The choice was driven by prioritizing higher-resolution structures with a low number of mutations in the crystallographic construct. Moreover, the choice of structure 4EIY for A_{2A} AR was made for a receptor co-crystallized with the inverse agonist ZM-241385, characterized by a 7-amino-2-(furan-2-yl)-[1,2,4]triazolo[1,5-*a*][1,3,5]triazine scaffold highly similar to that of the 5-amino-2-(furan-2-yl)-[1,2,4]triazolo[1,5-*c*]pyrimidin of the series of compounds reported here, suggesting the PDB structure, affected by induced-fit phenomena, to be a good candidate for docking studies.

No experimental structure is available for A_3 AR, and only agonist-bound G-protein-bound cryo-Electron Microscopy structures are available for A_{2B} AR [35,36]. To be consistent throughout the AR subtype comparison and avoid activation-state-dependent differences, the 3D structures of the A_{2B} and A_3 ARs were modeled using A_{2A} AR's (see alignment in Figure S1) and A_1 AR's (see alignment in Figure S2) inactive-state structures as templates, respectively, which provided the highest similarity to the couples A_1/A_3 (46% sequence identity, 65% sequence similarity) and A_{2A}/A_{2B} (45% sequence identity, 56% similarity).

Compounds **1**–**12** were docked at the four AR structures using a semi-rigid docking approach (ligand flexible/protein rigid), and one or more reasonable binding modes could be predicted just for compounds **8**–**12** at all receptor subtypes. Two reasonable binding modes were selected for almost all the compounds, prioritizing poses with a bidentate hydrogen bond with N6.55 considering the importance of this residue for antagonist and agonist binding [37,38].

In the case of hA_{2A} AR (Figure 1B, Video S2), the poses with the best electrostatic interaction potential resembled the X-ray conformation of the 7-amino-2-(furan-2-yl)-[1,2,4]triazolo[1,5-*a*][1,3,5]triazine portion of ZM-241385 (Figure S3). The exocyclic 5-amino group and nitrogen N3 are involved in a bidentate hydrogen bond with $N253^{6.55}$, and the aromatic pyrazolo-triazolo-pyrimidine scaffold participates in a pi–pi stacking with F168 on EL2. The furane ring points deep into the binding pocket, facing $H250^{6.52}$, where a T-shaped pi–pi interaction could occur. The alkyl group at position 8 points toward an area delimited by TM7/1/2/3 and EL2. The 5-amino group is further stabilized by a hydrogen bond with a glutamate on EL2 (E169), which is solvent exposed, but held in proximity to the top of the orthosteric pocket by an ionic interaction with $H264^{EL3}$ in most of the A_{2A} AR X-ray structures. A favorable electrostatic interaction potential is reported for E169 and compounds **8**–**12** (Video S2). An analogue situation was observed in the case of hA_{2B} AR (Figure 1D and Video S3).

Also, in the case of hA_1 AR, hA_{2B} AR, and hA_3 AR, a ZM-241385-like pose was generated for almost all compounds **8**–**12** (except compound **10** in the case of hA_1 AR and hA_3 AR) (Figure 1A,D,C and Videos S1, S3, and S4). In the case of hA_1 AR and hA_{2B} AR (Videos S1 and S3, Figure 1A,D), the key residues mentioned above for hA_{2A} AR are all conserved, with $F171^{EL2}$, $E172^{EL2}$, $H251^{6.52}$, and $N254^{6.55}$ of hA_1 AR and $F173^{EL2}$, $E174^{EL2}$, $H251^{6.52}$, and $N254^{6.55}$ of hA_{2B} AR acting like $F168^{EL2}$, $E169^{EL2}$, $H250^{6.52}$, and $N253^{6.55}$ of hA_{2A} AR. The electrostatic interaction between $E172^{EL2}$ of hA_1 AR and compounds **8**–**12** is not as evident as that in the case of hA_{2A} AR (Video S1), and no direct hydrogen bond was observed between the residues and the 5-amino group. However, this is due to the conformation of $E172^{EL2}$ in the X-ray structure, and alternative conformation might be expected in a dynamic solvent-exposed environment. Differently, in the case of hA_3 AR, the position of E169(hA_{2A})/E172(hA_1)/E174(hA_{2B}) is occupied by a hydrophobic residue, such as V169 (Figure S4). The favorable interaction between negatively charged and polar residues at this position with the free amino group at position 5 is, thus, missing. Moreover, a further difference can be noted: at position 6.52, instead of the Histidine that characterizes all the other subtypes, a less bulky Serine group ($S247^{6.52}$) is present that is incapable of making a T-shaped pi–pi interaction with the furane ring of the compounds. Together with this, a Serine residue ($S181^{5.42}$) also replaces an asparagine at position 5.42,

which is conserved in all the other AR subtypes, creating more space at the bottom of the binding pocket.

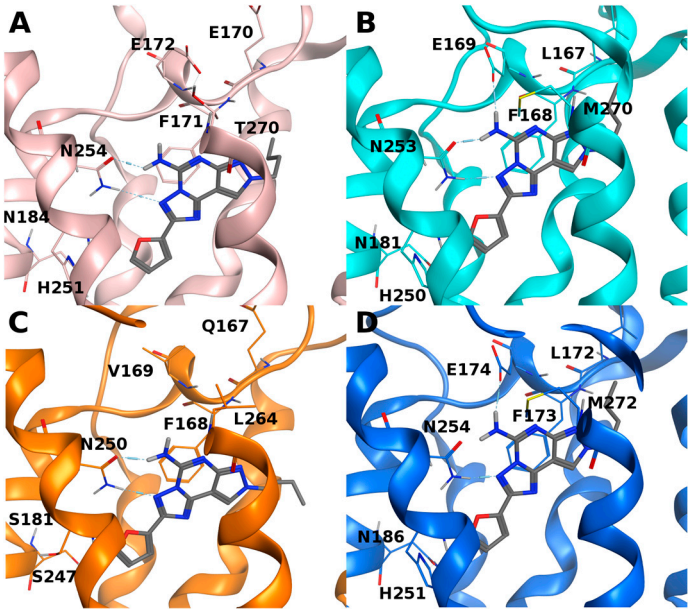

Figure 1. Docking pose of compound **11** (grey) at hA_1 (pink, (**A**)), hA_{2A} (cyan, (**B**)), hA_3 (orange, (**C**)), and hA_{2B} (blue, (**D**)) AR structures. The following receptor 3D structures were employed: experimental X-ray for hA_1 (PDB IDs: 5UEN) and hA_{2A} ARs (PDB IDs: 4EIY), homology models for hA_{2B} and hA_3 ARs (built on hA_{2A} and hA_1, respectively). A ZM-241385-like docking pose is displayed here.

An alternative reasonable binding mode can be observed for most of compounds **8**–**12** (Figure S5) which is highly ranked in terms of electrostatic interaction potential for the hA_1 and hA_3 ARs. The alternative conformation maintains the pi–pi stacking interaction with the phenylalanine on EL2 and the bidentate hydrogen bond with N6.55 on TM6. These poses engage N6.55 through the exocyclic amino group at position 5 and through N6 instead of N3. The 8-alkyl group faces the bottom of the binding pocket, while the furanyl group points toward the extracellular tip of TM2. This pose is also observed in the case of the hA_{2A} and hA_{2B} ARs but seems unfavored compared to the ZM-241385-like one because of a major inward position and consequent steric hindrance of TM2 as compared to the hA_1 and hA_3 ARs.

For compounds **1**–**7**, it was not possible to observe the aforementioned binding modes by conducting docking studies. A different approach has been adopted to relieve possible clashes of the receptors with the bulky groups at position N5. The bulkiest compound showing binding affinity at all four receptor subtypes, compound **4**, was selected to optimize the conformation of the binding pocket using induced-fit docking. The refined structures were then used for docking all compounds **1**–**7**. With this procedure, a ZM-241385-like pose was obtained for all the compounds at all four AR subtypes. The exocyclic 5-amino group and nitrogen N3 are engaged in a bidentate hydrogen bond (or approximate one) with N6.55, occupied by N254, N253, N254, and N250 in the hA_1, hA_{2A}, hA_{2B}, and hA_3 ARs, respectively, and the aromatic scaffold is involved in pi–pi interactions with F171, F168, F173, and F168 on EL2 (Figure 2A–D and Videos S1–S4). The N5 substituent increases the contacts with the hydrophobic residues in the binding site in all cases (Videos S1–S4). A hydrogen bond with E172/E169/E174 cannot occur in the case of these compounds with a consequent minor stabilization of the bound state in the hA_1, hA_{2A}, and hA_{2B} ARs. Moreover, the $E172^{EL2}$-$H264^{EL3}$ ionic interaction observed in hA_{2A} AR would also be disrupted, contributing to a loss of ligand stabilization.

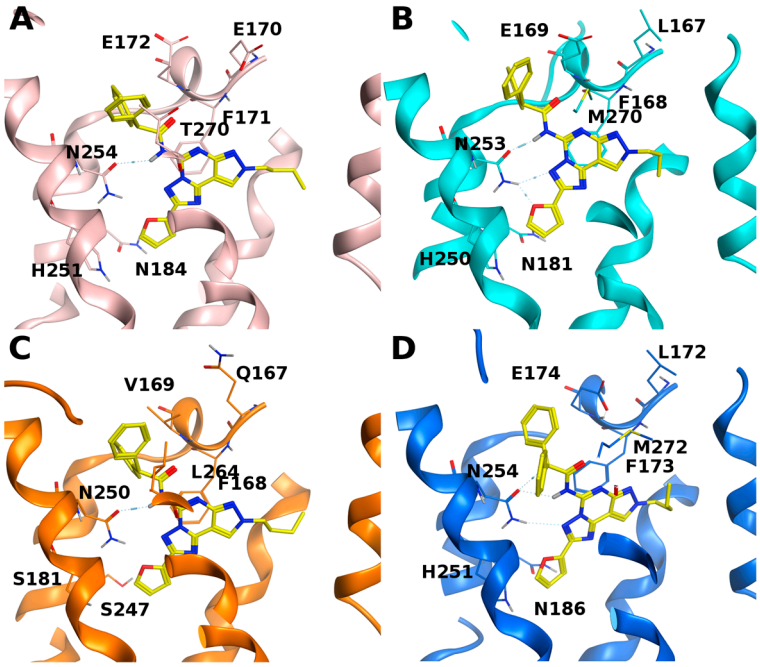

Figure 2. Docking pose of compound **4** (yellow) at hA_1 (pink, (**A**)), hA_{2A} (cyan, (**B**)), hA_3 (orange, (**C**)), and hA_{2B} (blue, (**D**)) AR structures. The following receptor 3D structures were employed: experimental X-ray for hA_1 (PDB IDs: 5UEN) and hA_{2A} ARs (PDB IDs: 4EIY), homology models for hA_{2B} and hA_3 ARs (built on hA_{2A} and hA_1, respectively). Structures were refined with induced-fit docking of compound **4** before re-docking it rigidly.

4. Discussion

In this work, twelve already-known pyrazolo-triazolo-pyrimidines were used to try to explain their profile of affinity and selectivity toward the four adenosine receptor subtypes through the identification of differences and/or similarities in the interaction patterns with the residues of the single subtypes. The four AR subtypes are characterized by high sequence identity in the orthosteric binding pocket; thus, the rationalization of ligand binding selectivity at different AR subtypes is not an easy task. It is reported that extracellular loops, especially EL2, might play a role in the ligand recognition process, especially in determining metastable binding sites along the ligand–receptor binding pathway [39–41]. In the current study, the contribution of EL2 or other ELs in the binding process has not been investigated, and, consequently, its role in affecting affinity and selectivity remains to be elucidated. The usage of docking, maintaining full rigidity on the protein structure (regardless of the use of an induced-fit docking technique), does not allow the investigation of the binding kinetics or metastable binding sites along the binding root. Molecular Dynamics (MD) simulations and Supervised Molecular Dynamics (SuMD) [42] could aid in this perspective, but a major limitation still takes place. For A_3 AR, there is still no availability of 3D experimental structures, and for hA_{2B} AR, the newly released cryo-EM structures in the active state have still not solved the coordinates of EL2 [35,36]. Considering that the reliability of loop modeling is poor, as long as an experimental 3D structure is not released to the scientific community, selectivity studies will still be limited.

Nevertheless, comparing possible binding final states can still be informative, at least to assess the capability of the competitive antagonists to be hosted in the orthosteric sites of ARs.

As mentioned before, the pyrazolo-triazolo-pyrimidines reported in this paper show binding capacity at all AR subtypes. Compounds **8**–**12**, characterized by a free amino group at position 5, show a binding affinity in the nanomolar range in the case of the hA_{2A}, hA_{2B}, and hA_1 ARs, while they reach an affinity of hundreds of nanomolar in the case of hA_3 AR. This trend is inverted for compounds acylated at position N5, with increased

affinity and selectivity for the hA_3 AR subtype. A hypothetical explanation consists of an increased stabilization of the N5 free amino compounds in the hA_1 and hA_{2A} ARs, thanks to a glutamate residue on EL2 (E172 for hA_1 and E169 hA_{2A}), in proximity of the binding pocket. This stabilizing effect is missing in the case of hA_3 AR, which bears the hydrophobic V169 at this position. Compounds acylated at position 5 would lose this stabilizing effect in the case of the hA_1 and hA_{2A} ARs and could hypothetically better fit the more hydrophobic environment created by V169. Unfortunately, this rationalization does not fit for the hA_{2B} AR subtype; even if it bears a glutamate residue on EL2 as with the hA_1 and hA_{2A} ARs, the binding data for the compounds acylated at position N5 are not so different from those for the compounds with a free amino group at the same position. Thus, this aspect should be further investigated, probably by exploring a hypothetical key role played by residues on EL2 and EL3.

Supplementary Materials: The following supporting information can be downloaded at: https://www.mdpi.com/article/10.3390/biom13111610/s1, Table S1: Adenosine receptor sequence identity and similarity; Figure S1: Alignment between hA_{2B} and hA_{2A} sequences for homology modeling; Figure S2: Alignment between hA_3 and hA_1 sequences for homology modeling; Figure S3: Binding mode of compound ZM-141385 at A_{2A} AR in X-ray structure 4EIY; Figure S4: Sequence alignment of all adenosine receptors; Figure S5: Alternative docking pose of compound **11** at hA_1, hA_{2A}, hA_{2B}, hA_3 ARs; Video S1: Docking poses of compounds **1**–**12** at hA_1 AR; Video S2: Docking poses of compounds **1**–**12** at hA_{2A} AR; Video S3: Docking poses of compounds **1**–**12** at hA_{2B} AR; Video S4: Docking poses of compounds **1**–**12** at hA_3 AR.

Author Contributions: Conceptualization, V.S., S.M., G.S. and S.F.; methodology, V.S., T.D.R. and K.-N.K.; validation, M.P., S.F. and V.S.; formal analysis, S.K., M.P. and V.S.; investigation, V.S.; data curation, K.-N.K., V.S., M.P. and S.F.; writing—original draft preparation, S.F., V.S. and G.S.; writing—review and editing, S.F., V.S. and S.M.; supervision, V.S. and S.F.; project administration, S.F. and V.S.; funding acquisition, S.M. and G.S. All authors have read and agreed to the published version of the manuscript.

Funding: This research received no external funding.

Institutional Review Board Statement: Not applicable.

Informed Consent Statement: Not applicable.

Data Availability Statement: The data presented in this study are available in this article (and Supplementary Material).

Acknowledgments: The molecular modeling work coordinated by S.M. was carried out with financial support from the University of Padova, Italy, and the Italian Ministry for University and Research (MIUR), Rome, Italy. S.M. is also very grateful to Chemical Computing Group for their scientific and technical partnership.

Conflicts of Interest: The authors declare no conflict of interest.

References

1. Borea, P.A.; Gessi, S.; Merighi, S.; Vincenzi, F.; Varani, K. Pharmacology of Adenosine Receptors: The State of the Art. *Physiol. Rev.* **2018**, *98*, 1591–1625. [CrossRef] [PubMed]
2. Burnstock, G. A basis for distinguishing two types of purinergic receptor. In *Cell Membrane Receptors for Drugs and Hormones: A Multidisciplinary Approach*; Bolis, L., Straub, R.W., Eds.; Raven Press: New York, NY, USA, 1978; pp. 107–118.
3. IJzerman, A.P.; Jacobson, K.A.; Müller, C.E.; Cronstein, B.N.; Cunha, R.A. International Union of Basic and Clinical Pharmacology. CXII: Adenosine Receptors: A Further Update. *Pharmacol. Rev.* **2022**, *74*, 340–372. [CrossRef] [PubMed]
4. Vincenzi, F.; Pasquini, S.; Contri, C.; Cappello, M.; Nigro, M.; Travagli, A.; Merighi, S.; Gessi, S.; Borea, P.A.; Varani, K. Pharmacology of Adenosine Receptors: Recent Advancements. *Biomolecules* **2023**, *13*, 1387. [CrossRef]
5. Jacobson, K.A.; Gao, Z.G. Adenosine receptors as therapeutic targets. *Nat. Rev. Drug Discov.* **2006**, *5*, 247–264. [CrossRef] [PubMed]
6. Chen, J.-F.; Eltzschig, H.K.; Fredholm, B.B. Adenosine receptors as drug targets—What are the challenges? *Nat. Rev. Drug Discov.* **2013**, *12*, 265–286. [CrossRef]
7. Effendi, W.I.; Nagano, T.; Kobayashi, K.; Nishimura, Y. Focusing on Adenosine Receptors as a Potential Targeted Therapy in Human Diseases. *Cells* **2020**, *9*, 785. [CrossRef]

8. Vincenzi, F.; Rotondo, J.C.; Pasquini, S.; Di Virgilio, F.; Varani, K.; Tognon, M. A_3 Adenosine and P2X7 Purinergic Receptors as New Targets for an Innovative Pharmacological Therapy of Malignant Pleural Mesothelioma. *Front. Oncol.* **2021**, *11*, 679285. [CrossRef]
9. Hammami, A.; Allard, D.; Allard, B.; Stagg, J. Targeting the adenosine pathway for cancer immunotherapy. *Semin. Immunol.* **2019**, *42*, 101304. [CrossRef]
10. Spinaci, A.; Buccioni, M.; Chang, C.; Dal Ben, D.; Francucci, B.; Lambertucci, C.; Volpini, R.; Marucci, G. Adenosine A_{2A} Receptor Antagonists: Chemistry, SARs, and Therapeutic Potential. In *Purinergic Receptors and Their Modulators. Topics in Medicinal Chemistry*; Colotta, V., Supuran, C.T., Eds.; Springer: Cham, Switzerland, 2023; Volume 41.
11. Coppi, E.; Cherchi, F.; Venturini, M.; Lucarini, E.; Corradetti, R.; Di Cesare Mannelli, L.; Ghelardini, C.; Pedata, F.; Pugliese, A. Therapeutic Potential of Highly Selective A_3 Adenosine Receptor Ligands in the Central and Peripheral Nervous System. *Molecules* **2022**, *27*, 1890. [CrossRef]
12. Gatta, F.; Del Giudice, M.; Borioni, A.; Borea, P.; Dionisotti, S.; Ongini, E. Synthesis of imidazo[1,2-*c*]pyrazolo[4,3-*e*]pyrimidines, pyrazolo[4,3-*e*]1,2,4-triazolo[1,5-*c*]pyrimidines and 1,2,4-triazolo[5,1-*i*]purines: New potent adenosine A_2 receptor antagonists. *Eur. J. Med. Chem.* **1993**, *28*, 569–576. [CrossRef]
13. Baraldi, P.G.; Cacciari, B.; Romagnoli, R.; Spalluto, G.; Monopoli, A.; Ongini, E.; Varani, K.; Borea, P.A. 7-Substituted 5-Amino-2-(2-furyl)pyrazolo[4,3-*e*]-1,2,4-triazolo[1,5-*c*]pyrimidines as A_{2A} Adenosine Receptor Antagonists: A Study on the Importance of Modifications at the Side Chain on the Activity and Solubility. *J. Med. Chem.* **2002**, *45*, 115–126. [CrossRef] [PubMed]
14. Redenti, S.; Ciancetta, A.; Pastorin, G.; Cacciari, B.; Moro, S.; Spalluto, G.; Federico, S. Pyrazolo[4,3-*e*][1,2,4]triazolo[1,5-*c*]pyrimidines and Structurally Simplified Analogs. Chemistry and SAR Profile as Adenosine Receptor Antagonists. *Curr. Top. Med. Chem.* **2016**, *16*, 3224–3257. [CrossRef] [PubMed]
15. Prencipe, F.; Da Ros, T.; Cescon, E.; Grieco, I.; Persico, M.; Spalluto, G.; Federico, S. Adenosine receptor ligands, probes, and functional conjugates: A 20-year hystory of pyrazolo[4,3-*e*][1,2,4]triazolo[1,5-*c*]pyrimidines (PTP). In *Purinergic Receptors and Their Modulators*; Colotta, V., Supuran, C.T., Eds.; Springer: Cham, Switzerland, 2023; ISBN 978-3-031-39724-0.
16. Glukhova, A.; Thal, D.M.; Nguyen, A.T.; Vecchio, E.A.; Jörg, M.; Scammells, P.J.; May, L.T.; Sexton, P.M.; Christopoulos, A. Structure of the adenosine A_1 receptor reveals the basis for subtype selectivity. *Cell* **2017**, *168*, 867–877. [CrossRef]
17. Liu, W.; Chun, E.; Thompson, A.A.; Chubukov, P.; Xu, F.; Katritch, V.; Han, G.W.; Roth, C.B.; Heitman, L.H.; Ijzerman, A.P.; et al. Structural basis for allosteric regulation of GPCRs by sodium ions. *Science* **2012**, *337*, 232–236. [CrossRef] [PubMed]
18. Chemical Computing Group ULC. *Molecular Operating Environment (MOE)*, version 2022.02; Chemical Computing Group ULC: Montreal, QC, Canada, 2023. Available online: https://www.chemcomp.com/ (accessed on 15 July 2023).
19. Katritch, V.; Fenalti, G.; Abola, E.E.; Roth, B.L.; Cherezov, V.; Stevens, R.C. Allosteric sodium in class A GPCR signaling. *Trends Biochem. Sci.* **2014**, *39*, 233–244. [CrossRef] [PubMed]
20. Margiotta, E.; Deganutti, G.; Moro, S. Could the presence of sodium ion influence the accuracy and precision of the ligand-posing in the human A_{2A} adenosine receptor orthosteric binding site using a molecular docking approach? Insights from Dockbench. *J. Comput. Aided Mol. Des.* **2018**, *32*, 1337–1346. [CrossRef] [PubMed]
21. Jacobson, M.P.; Friesner, R.A.; Xiang, Z.; Honig, B. On the role of the crystal environment in determining protein side-chain conformations. *J. Mol. Biol.* **2002**, *320*, 597–608. [CrossRef]
22. Jacobson, M.P.; Pincus, D.L.; Rapp, C.S.; Day, T.J.F.; Honig, B.; Shaw, D.E.; Friesner, R.A. A hierarchical approach to all-atom protein loop prediction. *Proteins* **2004**, *55*, 351–367. [CrossRef]
23. Ballesteros, J.A.; Weinstein, H. [19] Integrated methods for the construction of three-dimensional models and computational probing of structure-function relations in G protein-coupled receptors. In *Receptor Molecular Biology*; Methods in Neurosciences; Elsevier: Amsterdam, The Netherlands, 1995; Volume 25, pp. 366–428.
24. Pándy-Szekeres, G.; Munk, C.; Tsonkov, T.M.; Mordalski, S.; Harpsøe, K.; Hauser, A.S.; Bojarski, A.J.; Gloriam, D.E. GPCRdb in 2018: Adding GPCR structure models and ligands. *Nucleic Acids Res.* **2018**, *46*, D440–D446. [CrossRef]
25. Friesner, R.A.; Banks, J.L.; Murphy, R.B.; Halgren, T.A.; Klicic, J.J.; Mainz, D.T.; Repasky, M.P.; Knoll, E.H.; Shelley, M.; Perry, J.K.; et al. Glide: A new approach for rapid, accurate docking and scoring. 1. Method and assessment of docking accuracy. *J. Med. Chem.* **2004**, *47*, 1739–1749. [CrossRef]
26. Sherman, W.; Day, T.; Jacobson, M.P.; Friesner, R.A.; Farid, R. Novel procedure for modeling ligand/receptor induced fit effects. *J. Med. Chem.* **2006**, *49*, 534–553. [CrossRef]
27. Pettersen, E.F.; Goddard, T.D.; Huang, C.C.; Couch, G.S.; Greenblatt, D.M.; Meng, E.C.; Ferrin, T.E. UCSF Chimera—A visualization system for exploratory research and analysis. *J. Comput. Chem.* **2004**, *25*, 1605–1612. [CrossRef]
28. Michielan, L.; Bolcato, C.; Federico, S.; Cacciari, B.; Bacilieri, M.; Klotz, K.-N.; Kachler, S.; Pastorin, G.; Cardin, R.; Sperduti, A.; et al. Combining selectivity and affinity predictions using an integrated Support Vector Machine (SVM) approach: An alternative tool to discriminate between the human adenosine A_{2A} and A_3 receptor pyrazolo-triazolo-pyrimidine antagonists binding sites. *Bioorg. Med. Chem.* **2009**, *17*, 5259–5274. [CrossRef]
29. Michielan, L.; Stephanie, F.; Terfloth, L.; Hristozov, D.; Cacciari, B.; Klotz, K.; Spalluto, G.; Gasteiger, J.; Moro, S. Exploring Potency and Selectivity Receptor Antagonist Profiles Using a Multilabel Classification Approach: The Human Adenosine Receptors as a Key Study. *J. Chem. Inf. Model.* **2009**, *49*, 2820–2836. [CrossRef]

30. Klotz, K.-N.; Hessling, J.; Hegler, J.; Owman, C.; Kull, B.; Fredholm, B.B.; Lohse, M.J. Comparative pharmacology of human adenosine receptor subtypes—Characterization of stably transfected receptors in CHO cells. *Naunyn Schmiedebergs Arch. Pharmacol.* **1998**, *357*, 1–9. [CrossRef]
31. De Lean, A.; Hancock, A.A.; Lefkowitz, R.J. Validation and statistical analysis of a computer modeling method for quantitative analysis of radioligand binding data for mixtures of pharmacological receptor subtypes. *Mol. Pharmacol.* **1982**, *21*, 5–16.
32. Lohse, M.J.; Lenschow, V.; Schwabe, U. Two affinity states of Ri adenosine receptors in brain membranes. Analysis of guanine nucleotide and temperature effects on radioligand binding. *Mol. Pharmacol.* **1984**, *26*, 1–9.
33. Baraldi, P.G.; Cacciari, B.; Romagnoli, R.; Spalluto, G.; Moro, S.; Klotz, K.N.; Leung, E.; Varani, K.; Gessi, S.; Merighi, S.; et al. Pyrazolo[4,3-*e*]1,2,4-triazolo[1,5-*c*]pyrimidine derivatives as highly potent and selective human A_3 adenosine receptor antagonists: Influence of the chain at the N^8 pyrazole nitrogen. *J. Med. Chem.* **2000**, *43*, 4768–4780. [CrossRef]
34. Klotz, K.N.; Cristalli, G.; Grifantini, M. Photoaffinity labeling of A1-adenosine receptors. *J. Biol. Chem.* **1985**, *260*, 14659–14664. [CrossRef]
35. Chen, Y.; Zhang, J.; Weng, Y.; Xu, Y.; Lu, W.; Liu, W.; Liu, M.; Hua, T.; Song, G. Cryo-EM structure of the human adenosine A_{2B} receptor-G_s signaling complex. *Sci. Adv.* **2022**, *8*, eadd3709. [CrossRef]
36. Cai, H.; Xu, Y.; Guo, S.; He, X.; Sun, J.; Li, X.; Li, C.; Yin, W.; Cheng, X.; Jiang, H.; et al. Structures of adenosine receptor A_{2B}R bound to endogenous and synthetic agonists. *Cell Discov.* **2022**, *8*, 140. [CrossRef] [PubMed]
37. Kim, J.; Wess, J.; van Rhee, A.M.; Schöneberg, T.; Jacobson, K.A. Site-directed mutagenesis identifies residues involved in ligand recognition in the human A_{2a} adenosine receptor. *J. Biol. Chem.* **1995**, *270*, 13987–13997. [CrossRef]
38. Gao, Z.-G.; Chen, A.; Barak, D.; Kim, S.-K.; Müller, C.E.; Jacobson, K.A. Identification by site-directed mutagenesis of residues involved in ligand recognition and activation of the human A_3 adenosine receptor. *J. Biol. Chem.* **2002**, *277*, 19056–19063. [CrossRef]
39. Peeters, M.C.; van Westen, G.J.P.; Li, Q.; Ijzerman, A.P. Importance of the extracellular loops in G protein-coupled receptors for ligand recognition and receptor activation. *Trends Pharmacol. Sci.* **2011**, *32*, 35–42. [CrossRef] [PubMed]
40. Wheatley, M.; Wootten, D.; Conner, M.T.; Simms, J.; Kendrick, R.; Logan, R.T.; Poyner, D.R.; Barwell, J. Lifting the lid on GPCRs: The role of extracellular loops. *Br. J. Pharmacol.* **2012**, *165*, 1688–1703. [CrossRef]
41. De Filippo, E.; Hinz, S.; Pellizzari, V.; Deganutti, G.; El-Tayeb, A.; Navarro, G.; Franco, R.; Moro, S.; Schiedel, A.C.; Müller, C.E. A_{2A} and A_{2B} adenosine receptors: The extracellular loop 2 determines high (A_{2A}) or low affinity (A_{2B}) for adenosine. *Biochem. Pharmacol.* **2020**, *172*, 113718. [CrossRef] [PubMed]
42. Cuzzolin, A.; Sturlese, M.; Deganutti, G.; Salmaso, V.; Sabbadin, D.; Ciancetta, A.; Moro, S. Deciphering the Complexity of Ligand-Protein Recognition Pathways Using Supervised Molecular Dynamics (SuMD) Simulations. *J. Chem. Inf. Model.* **2016**, *56*, 687–705. [CrossRef]